University Library



A gateway to Melbourne's research publications

Minerva Access is the Institutional Repository of The University of Melbourne

Author/s:
King, MJ;Wheeler, MC;Lane, TP

Title:
5-day-wave interactions with tropical precipitation in CMIP5 models

Date:
2016-12

Citation:
King, M. J., Wheeler, M. C. & Lane, T. P. (2016). 5-day-wave interactions with tropical precipitation in CMIP5 models. Journal of Climate, 29 (23), pp.8611-8624. https://doi.org/10.1175/JCLI-D-16-0190.1.

Persistent Link:
https://hdl.handle.net/11343/214002

5-Day-Wave Interactions with Tropical Precipitation in CMIP5 Models

MALCOLM J. KING

School of Earth Sciences, and ARC Centre of Excellence for Climate System Science, University of Melbourne, Melbourne, Victoria, Australia

MATTHEW C. WHEELER

Bureau of Meteorology, Melbourne, Victoria, Australia

TODD P. LANE

School of Earth Sciences, and ARC Centre of Excellence for Climate System Science, University of Melbourne, Melbourne, Victoria, Australia

(Manuscript received 3 March 2016, in final form 21 August 2016)

ABSTRACT

The 5-day Rossby–Haurwitz wave is unlike other large-scale wave modes that interact with tropical rainfall in that associated rainfall presents as a modulation of localized areas of rainfall instead of propagating with the wave. This form of wave-modulated convective organization in climate models has received little attention. This study investigates the simulation of interactions between the 5-day wave and tropical convection in 30 models from phase 5 of the Coupled Model Intercomparison Project (CMIP5) and compares these with the interaction diagnosed from ERA-Interim and TRMM precipitation data. Models simulate the dry dynamics of the 5-day wave well, with realistic coherences between upper- and lower-tropospheric winds, as well as magnitudes and geographic distribution of wave wind anomalies being close to observations. The models consistently display significant coherences between 5-day-wave zonal winds and precipitation but perform less well at simulating the spatial distribution and magnitude of precipitation anomalies. For example, a third of the models do not reproduce significant observed anomalies near the Andes, and the best-performing model simulates only 38% of the observed variance over the tropical Andes and 24% of the observed variance over the Gulf of Guinea. Models with higher resolution perform better in simulating the magnitude of the Andean rainfall anomalies, but there is no similar relationship over the Gulf of Guinea. The evidence therefore suggests that the simulated interaction is mostly one way only, with the wave dynamics forcing the precipitation variations on the 5-day time scale.

1. Introduction

The organization of tropical convection in space and time is important for how it interacts with the global circulation and the climate system in general. It is thus important that climate models reflect observed patterns of organization in order to accurately simulate climate processes. On time scales between days and seasons (1–90 days), the organization of tropical convection is dominated by the convectively coupled equatorial waves (CCEWs; Kiladis et al. 2009) and the Madden–Julian oscillation (MJO; Madden and Julian 1972a; Zhang 2005). These modes consist of large-scale coupled dynamic and convective fields that propagate together, and as such, the propagation and characteristics of these modes are strongly governed by the interactions between convection and the large-scale dynamic fields. These wave modes are important in weather systems such as monsoons (Yasunari 1979; Hendon and Liebmann 1990), tropical cyclones (Liebmann et al. 1994; Bessafi and Wheeler 2006), and, through teleconnections, extratropical

Supplemental information related to this paper is available at the Journals Online website: http://dx.doi.org/10.1175/JCLI-D-16-0190.s1.

Corresponding author address: Malcolm King, School of Earth Sciences, University of Melbourne, Elgin St. and Swanston St., Melbourne VIC 3010, Australia.
E-mail: malcolmk@student.unimelb.edu.au

DOI: 10.1175/JCLI-D-16-0190.1

© 2016 American Meteorological Society

precipitation systems (Jones 2000). However, current climate models have difficulty simulating these modes of organized tropical convection (Lin et al. 2006; Straub et al. 2010; Hung et al. 2013).

Evidence also exists for another atmospheric wave mode, the "5-day wave," which significantly interacts with tropical convection (Hendon and Wheeler 2008; King et al. 2015). The 5-day wave is the gravest symmetrical free Rossby wave (or Rossby–Haurwitz wave) with zonal wavenumber 1. The free Rossby waves are a class of external normal modes of the atmosphere, characterized by their barotropic vertical structure, westward propagation relative to the local flow, and lower frequencies compared to the other class of external modes (i.e., the free gravity waves; Salby 1984; Madden 2007).

The wind and geopotential anomalies associated with the 5-day wave propagate westward with a period of between 4 and 6 days (Madden and Julian 1972b), but unlike the MJO and CCEWs, the convective fields associated with the 5-day wave do not appear to propagate with the wave and are instead localized to a few locations in the tropics, specifically the lower slopes of the tropical Andes and over the Gulf of Guinea near West Africa, where it can modulate rainfall by up to 4 mm day^{-1} and is a key source of submonthly rainfall variability (King et al. 2015). Over the equatorial belt between central Africa and the Andes, the wave modulates observed precipitation by around 5% and observed lightning by 7% relative to the mean (Burpee 1976).

Unlike for the CCEWs and the MJO, global circulation models have featured semirealistic 5-day-wave signatures in geopotential and wind for at least 30 years (Hayashi and Golder 1983; Hamilton 1987; Manzini and Hamilton 1993), and higher-wavenumber Rossby–Haurwitz waves have been suggested as a tool to test the dynamical cores of climate models (Williamson et al. 1992). Model-based studies investigating the excitation of the 5-day wave have suggested that latent heat release in the tropics plays a crucial role in exciting this and other atmospheric normal modes (Salby and Garcia 1987; Garcia and Salby 1987; Hamilton 1987; Miyoshi and Hirooka 1999), although the lowest meridional mode has also been identified in dry climate models (Potter et al. 2014). Despite this, it is not currently known how well the interaction between the 5-day wave and tropical convection is simulated in modern climate models, and examining how models represent this little-investigated interaction between dynamics and convection allows for greater understanding of the quality of tropical convective processes in atmospheric models.

This study investigates the interaction between tropical convection and the 5-day wave in 30 of the CMIP5 climate models, utilizing two complementary techniques described in King et al. (2015). The remainder of the paper is organized as follows. Section 2 describes the data and methodology used in this paper. Section 3 presents the space–time power and coherence-squared spectra of tropospheric zonal winds and precipitation from the models, as well as the 5-day-wave wind and precipitation composite structures. Section 4 will discuss issues about the interaction between the 5-day wave and tropical convection arising from the model results presented in section 3, and finally, conclusions are presented in section 5.

2. Data and methods

a. Climate model and validation datasets

Representations of the interaction between the 5-day wave and tropical convection are investigated using four variables: precipitation, which is used as a marker of large-scale convection; 250-hPa zonal wind, which is used to assess upper-tropospheric dynamics; and 850-hPa zonal and meridional winds, which are used to assess lower-tropospheric dynamics.

The climate models assessed are 30 members of phase 5 of the Coupled Model Intercomparison Project (CMIP5), as listed in Table 1. Daily winds and precipitation values were obtained from the models' historical simulations for the period 1980–2005 for all models but HadGEM2-CC, where the data were only available for the period December 1979–November 2005 and were obtained and analyzed over this period for this model only. Where a climate model had an ensemble of many members, data from the r1i1p1 ensemble member were analyzed, as this member was available for all models.

Evaluation was performed using wind data from the ERA-Interim dataset (ECMWF 2009; Dee et al. 2011) and precipitation from the Tropical Rainfall Measuring Mission (TRMM) 3B42 version 7 dataset (Huffman et al. 2007; TRMM 2011). These data were taken from the period 1998–2012 and thus have a shorter temporal extent than the model data.

b. Coherence-squared spectra

A coherence spectral analysis was performed for each of the 30 models, computed for pairs of 850-hPa/250-hPa zonal wind and 850-hPa zonal wind/precipitation, in order to determine the existence of both the 5-day wave and an interaction between the wave and tropical convection on a global scale in the models as well as allowing a rough metric of how "strong" the interaction is. The procedure utilized is similar to that used in previous studies (e.g., Hendon and Wheeler 2008; Yasunaga and Mapes 2012; King et al. 2015).

TABLE 1. List of the CMIP5 models used in this study along with their native horizontal resolution near the equator and references providing further model details. Only one historical simulation ensemble member per model was used in this study. (Expansions of acronyms are available online at http://www.ametsoc.org/PubsAcronymList.)

Model	Horizontal resolution (lat × lon)	Reference
ACCESS1.0	1.25° × 1.88°	Bi et al. (2013)
ACCESS1.3	1.25° × 1.88°	Bi et al. (2013)
BCC_CSM1.1	2.79° × 2.81°	Xin et al. (2013)
BCC_CSM1.1(m)	1.12° × 1.13°	Xin et al. (2013)
BNU-ESM	2.79° × 2.81°	Ji et al. (2014)
CanESM2	2.79° × 2.81°	Arora et al. (2011)
CMCC-CESM	3.71° × 3.75°	Scoccimarro et al. (2011)
CMCC-CM	0.75° × 0.75°	Scoccimarro et al. (2011)
CMCC-CMS	1.87° × 1.88°	Scoccimarro et al. (2011)
CNRM-CM5	1.40° × 1.41°	Voldoire et al. (2013)
CSIRO Mk3.6.0	1.87° × 1.88°	Rotstayn et al. (2010)
FGOALS-g2	2.79° × 2.81°	Zhou et al. (2013)
GFDL CM3	2.00° × 2.50°	Donner et al. (2011)
GFDL-ESM2G	2.02° × 2.50°	Dunne et al. (2012)
GFDL-ESM2M	2.02° × 2.50°	Dunne et al. (2012)
HadCM3	2.50° × 3.75°	Collins et al. (2001)
HadGEM2-CC	1.25° × 1.88°	Martin et al. (2011)
INM-CM4.0	1.50° × 2.00°	Volodin et al. (2010)
IPSL-CM5A-LR	1.90° × 3.75°	Dufresne et al. (2013)
IPSL-CM5A-MR	1.27° × 2.50°	Dufresne et al. (2013)
IPSL-CM5B-LR	1.90° × 3.75°	Dufresne et al. (2013)
MIROC-ESM	2.79° × 2.81°	Watanabe et al. (2010)
MIROC-ESM-CHEM	2.79° × 2.81°	Watanabe et al. (2010)
MIROC4h	0.56° × 0.56°	Sakamoto et al. (2012)
MIROC5	1.40° × 1.41°	Watanabe et al. (2010)
MPI-ESM-LR	1.87° × 1.88°	Giorgetta et al. (2013)
MPI-ESM-P	1.87° × 1.88°	Giorgetta et al. (2013)
MRI-CGCM3	1.12° × 1.13°	Yukimoto et al. (2012)
MRI-ESM1	1.12° × 1.13°	Adachi et al. (2013)
NorESM1-M	1.90° × 2.50°	Bentsen et al. (2013)

Data for each variable are first partitioned into equatorially symmetric and antisymmetric components for each latitude up to 15° from the equator, and analysis is only performed upon the symmetric data. The symmetric component datasets are then broken into a series of 96-day segments, each starting a day later than the previous so that adjacent segments overlap by 95 days. Each individual segment is detrended and tapered to zero over the first and last 5 days by a split cosine-tapered rectangular window. The segmented data are then Fourier transformed in time at each longitude and latitude, Fourier transformed in longitude at each frequency and latitude, and used to calculate spectral power and copower for each segment. These are then averaged over all segments and latitudes. To improve the display, the spectral power estimates are smoothed in frequency by a 1–2–1 running mean filter. This results in a reduction of effective bandwidth but not to an extent where the 5-day wave is no longer identifiable. Westward-propagating features are displayed as negative wavenumbers and eastward as positive.

Existence of a relationship in the spectral space is determined by testing against the null hypothesis of no relationship using the method in von Storch and Zwiers (1999), with the degrees of freedom (dof) estimated by the following:

$$\begin{aligned}\text{dof} = {} & 2(\text{amplitude and phase}) \times \text{years of data} \\ & \times 360(\text{lowest value of days per year for the models}) \\ & \times 3(\text{1-2-1 filter})/96(\text{size of segment}).\end{aligned}$$

This gives a value of at least 585 dof for the climate models and 342 dof for evaluation data.

c. *Space–time filtering and lagged-regression composites*

Lagged-regression composites based on a filtered zonal wind time series are used to determine the geographical spread and magnitude of the precipitation signals in models relative to those in observations. Following King et al. (2015), an index time series of the 5-day wave for each model was obtained by first filtering 850-hPa zonal wind anomalies for westward wavenumber 1 and periods between 4 and 6 days. Then the latitudinal average of the

filtered data was taken between 7.5°S and 7.5°N at 0° longitude, forming a reference time series against which raw 850-hPa zonal winds and precipitation were regressed.

As in King et al. (2015), regression was only performed for time intervals where the variance in a 19-day window of the reference time series was greater than the total variance of the reference time series so as to minimize the effect of periods of low 5-day-wave magnitude on the composites. The window size was chosen to be 19 days because it is just larger than 3 times the longest filtered period, though the results are relatively insensitive to the window size.

Statistical significance of the regressed anomalies against a null hypothesis of no anomaly was determined through a Student's t test. When directly comparing average anomalies in a region, the models and observational data were regridded to the same resolution as CMCC-CESM, the model with the lowest spatial resolution of 3.71° × 3.75°, before the composites were generated so that data could be more fairly compared.

3. Results

a. Spectral analysis

Figure 1 shows the raw symmetric wavenumber–frequency spectra of 850-hPa zonal winds and precipitation for the ERA-Interim and TRMM datasets as well as three representative CMIP5 models: ACCESS1.3, MPI-ESM-P, and INM-CM4.0. INM-CM4.0 is presented as it shows the most coherent 5-day-wave signals (as can be seen in Fig. 3), MPI-ESM-P is presented as it shows coherences between 5-day-wave zonal winds and precipitation close to that in observations, and ACCESS1.3 is shown as it is the most recent coupled model from Australian modeling groups. Similar precipitation spectra for other CMIP5 models can be found in Fig. 3 of Hung et al. (2013) and zonal wind spectra in Fig. 4 of Lott et al. (2014) although for lower-stratospheric zonal winds instead of lower-tropospheric zonal winds. The CMIP models tend to show increased variance in high-frequency zonal winds (above 0.1 cycles per day) compared to the ERA-Interim dataset, although INM-CM4.0 (Fig. 1g) has reduced variance in high-frequency zonal winds. Despite this, all models including INM-CM4.0 have greater raw variance in 850-hPa zonal winds at the 5-day range than seen in ERA-Interim. On the other hand, CMIP5 models tend to underrepresent precipitation variation at frequencies at and above 0.2 cycles per day, including the 5-day-wave range, but overstate westward-propagating low-frequency rainfall variance compared to TRMM.

The coherence spectrum between equatorially symmetric 850- and 250-hPa ERA-Interim zonal winds, shown in Fig. 2a, has the 5-day wave appearing as a peak in the coherence-squared statistic of ~0.4 at westward (i.e., negative) wavenumber 1. Also apparent are higher-wavenumber Rossby–Haurwitz waves, which appear at westward wavenumbers 2–5 with periods from ~8.5 to 3.5 days. The coherence-squared peaks for these observed waves well match the plotted theoretical dispersion curve for the $n = 1$ Rossby–Haurwitz wave, assuming a shallow-water equivalent depth of 10 km and an effective advective zonal wind from midlatitude background winds of $15\,\mathrm{m\,s^{-1}}$ (Kasahara 1980). This result is consistent with the results of Hendon and Wheeler (2008) and King et al. (2015).

Another prominent peak in the ERA-Interim zonal wind coherence spectrum of Fig. 2a is that of the MJO, with a coherence-squared of greater than 0.5 at eastward wavenumber 1 and periods of 30–80 days. The upper- and lower-tropospheric wind fields are out of phase for the MJO (downward-pointing vector) but roughly in phase (upward-pointing vector) for the Rossby–Haurwitz waves, confirming their well-known baroclinic and barotropic vertical structures, respectively. In addition, relatively high coherence-squared values occur for both dry and convectively coupled Kelvin waves at eastward-propagating wavenumbers 1–5, with the convectively coupled equatorial Kelvin waves at lower frequencies (periods of 5–20 days) and the dry Kelvin waves at higher frequencies (periods of less than about 4 days).

In the coherence spectrum between symmetric 850-hPa ERA-Interim zonal wind and TRMM 3B42 precipitation (Fig. 2b), the coherence-squared peaks of the waves that involve a strong interaction with convection remain strong or strengthen (in comparison to the peaks in Fig. 2a). For example, the peaks of the MJO and convectively coupled Kelvin waves appear strong and extend to higher zonal wavenumbers. On the other hand, the coherence signals for the purely dry waves such as the dry Kelvin wave disappear. For the $n = 1$ Rossby–Haurwitz wave, the coherence peaks for all wavenumbers disappear except for westward wavenumber 1, corresponding to the 5-day wave, and the level of coherence is weaker than not only that displayed by the MJO but also that of the convectively coupled Kelvin and equatorial Rossby waves. Despite this, the 5-day wave still displays the strongest coherence between any large-scale westward-propagating disturbance and precipitation at time scales between 2.5 and 10 days. The phase relationship between lower-tropospheric wind and precipitation for the 5-day wave is similar to that observed for the MJO and the convectively coupled Kelvin waves, with enhanced precipitation leading westerly wind anomalies by a quarter cycle.

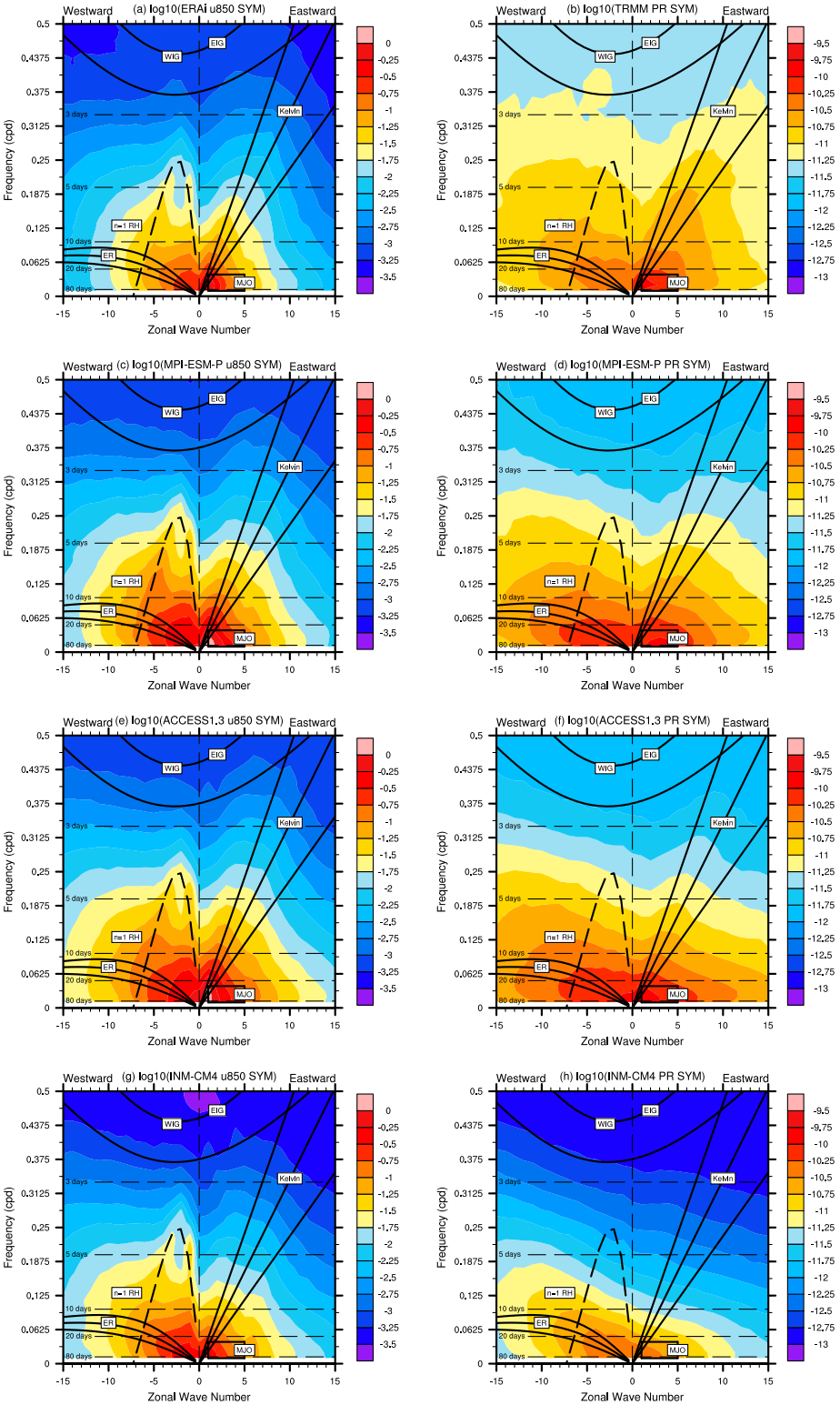

FIG. 1. Space–time power spectra of (left) 850-hPa zonal winds and (right) precipitation from (a),(b) ERA-Interim and TRMM 3B42, and the (c),(d) MPI-ESM-P, (e),(f) ACCESS1.3, and (g),(h) INM-CM4.0 climate models. Solid dispersion curves are shown for the Kelvin wave, $n = 1$ equatorial Rossby (ER) wave, $n = 1$ westward inertia-gravity (WIG), and $n = 1$ eastward inertia-gravity (EIG) waves with equivalent depths of 12, 25, and 50 m; a dashed dispersion curve is shown for the $n = 1$ Rossby–Haurwitz ($n = 1$ RH) wave with equivalent depth of 10 km assuming background zonal flow of 15 m s^{-1}.

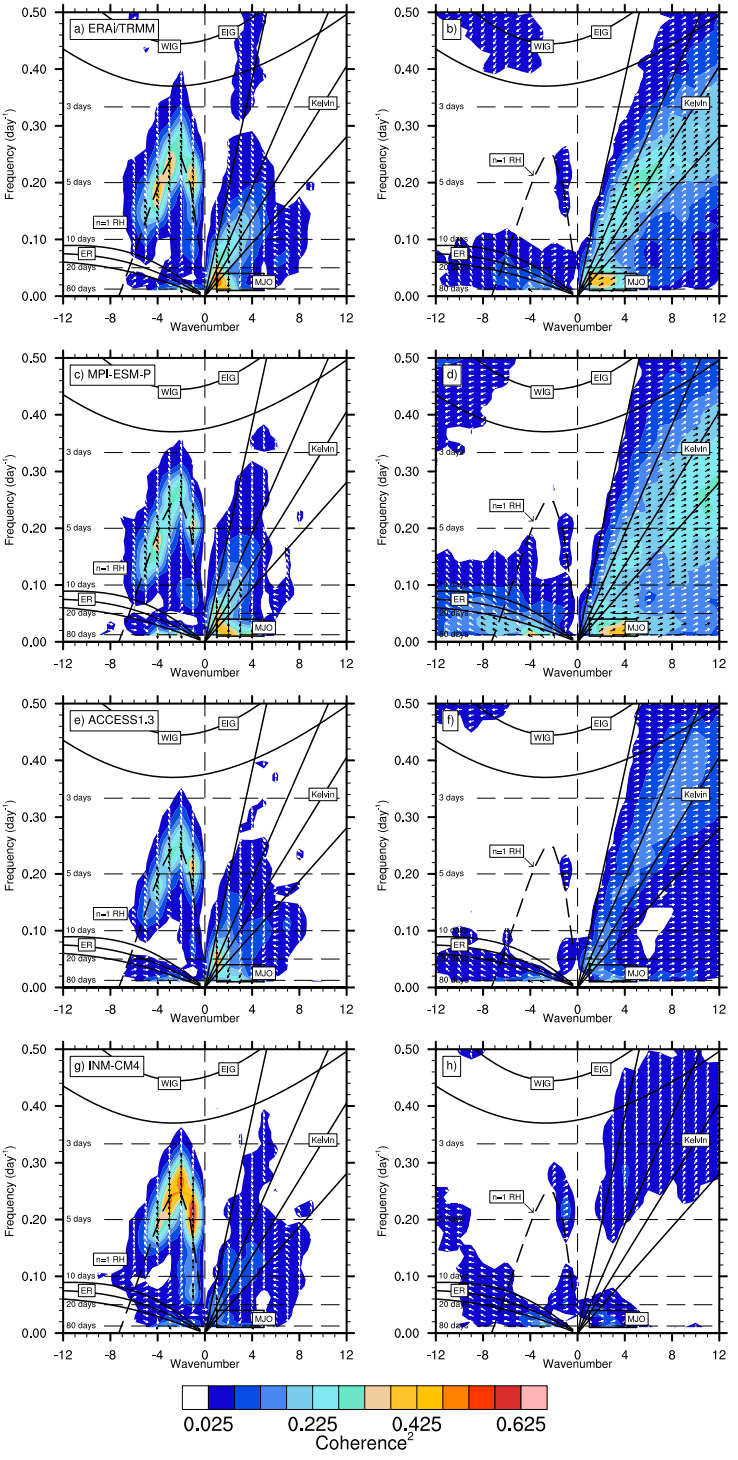

FIG. 2. Space–time spectrum of coherence squared (contours) and phase (vectors) for symmetric components of (left) 250- and 850-hPa zonal winds and (right) precipitation and 850-hPa zonal winds, from (a),(b) ERA-Interim and TRMM 3B42 data, (c),(d) MPI-ESM-P, (e),(f) ACCESS1.3, and (g),(h) INM-CM4.0. The first contour, at 0.025, is significant at the 99% level. Phase vectors pointing upward denote the two fields being in phase, and downward-pointing vectors denote an out-of-phase relationship. Vectors to the left and right indicate that upper-tropospheric zonal winds and precipitation precede and lag lower-tropospheric zonal winds, respectively. Dispersion curves are as in Fig. 1, with an additional Kelvin wave dispersion curve at an equivalent depth of 200 m.

These coherence spectra can be compared with those from the three representative CMIP5 climate models in Figs. 2c–h (and for the other 27 CMIP5 models in Fig. 1 of the supplemental material) and with the average and maximum coherence-squared values at westward wavenumber 1 in the 4–6-day range for all 30 models in Fig. 3. For the MJO, the CMIP5 climate models investigated here poorly simulate the coherence between upper- and lower-tropospheric winds (Fig. 2, left), in line with the well-known difficulties in simulating the MJO (Hung et al. 2013). The model simulations both underrepresent the level of coherence seen in observational data and place the MJO coherence signal at a higher frequency than what is observed.

The models simulate the coherences between the two levels of zonal winds associated with the $n = 1$ Rossby–Haurwitz waves reasonably well, with all models placing the peak coherence for these waves near the correct frequency for wavenumbers 1–5. While individual model coherences for the free Rossby waves vary from below that observed (as in ACCESS1.3; Fig. 2e) to above that observed (as in INM-CM4.0; Fig. 2g), the values in Fig. 3a show that the model 5-day-wave wind coherences vary around that seen in the observations, with no model having a peak coherence-squared in the 5-day-wave range less than 0.32. This is in line with previous studies showing general circulation models being able to realistically simulate the 5-day wave, even without moist convective forcing (Hayashi and Golder 1983; Miyoshi and Hirooka 1999; Potter et al. 2014).

The climate models also perform better at accurately simulating the coherence between zonal winds and precipitation associated with the 5-day wave than they do with features such as the MJO and convectively coupled Kelvin waves (Fig. 2, right column). Models strongly underrepresent the strength of the interaction between the zonal winds and precipitation for the MJO and Kelvin waves, with even one of the models closest to the reanalysis (MPI-ESM-P; Fig. 2d) having reduced coherence between zonal wind anomalies and precipitation in the MJO and Kelvin waves up to zonal wavenumber 8.

The models also tend to separate the MJO wind and precipitation coherence signal into two parts: a low-frequency, wavenumber-2–5 signal and a higher-frequency, wavenumber-1–2 signal. The low-frequency component is at a frequency below that of the observed MJO (Fig. 2b) and tends to extend more toward higher wavenumbers; the higher-frequency component is at a slightly higher frequency than the observed MJO and seems to be more coincident with the low-wavenumber Kelvin wave dispersion relationship.

Despite the relatively poor performance the models have in simulating the coherence between zonal wind and precipitation associated with the MJO and Kelvin waves, all the models simulate significant coherences between 850-hPa zonal winds and precipitation for the 5-day wave, which are close to the observed coherence. However, unlike the upper- and lower-tropospheric zonal wind coherence, there is a greater spread of maximum coherence values between the models relative to the maximum coherence value seen in observations (Fig. 3b), with values ranging from around double that seen in observed data (HadCM3 and INM-CM4.0) to values around half of that observed (GFDL CM3 and IPSL-CM5A-LR). There is also a less consistent relationship between the maximum and average coherence-squared values in the 5-day range, suggesting that some models have a more peaked coherence signal than others. Curiously, INM-CM4.0 has the strongest wind–precipitation coherence for the 5-day wave but

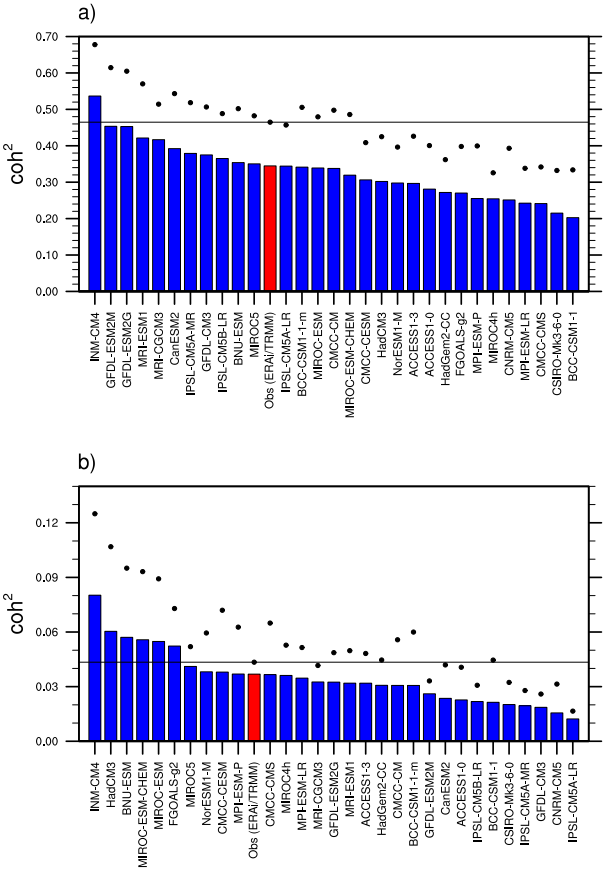

FIG. 3. Average (bars) and maximum (dots) coherence squared at westward zonal wavenumber 1 and with a period of 4–6 days between (a) 850- and 250-hPa zonal winds and (b) 850-hPa zonal winds and precipitation for observations and the CMIP5 models. The average coherence squared for the observations is in red, and a reference line is located at maximum coherence of the observations.

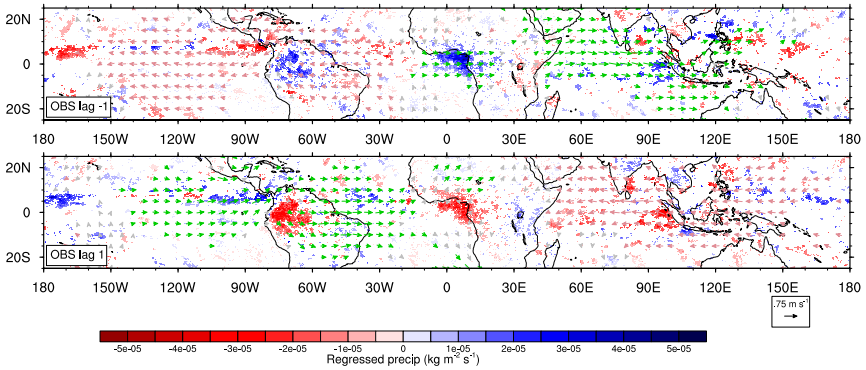

FIG. 4. Composite 850-hPa horizontal wind (vectors) and precipitation anomalies (shading) from ERA-Interim and TRMM 3B42 associated with the 5-day wave, at 1 day (top) before and (bottom) after maximum wave amplitude at 0°, 0°. Values are scaled by two standard deviations of wave amplitude. Values shown are significant at the 95% level.

some of the weakest coherence values for the convectively coupled Kelvin waves and the MJO (Fig. 2h).

b. *Composites*

Consistent with the results of King et al. (2015), the observed composite wind field associated with the 5-day wave (Fig. 4) closely replicates that predicted by theory (Elbern and Speth 1993), with a zonal wavenumber-1 structure in zonal wind anomalies along the equator that propagates westward by about 150° longitude in two days. Reductions in 850-hPa wind anomaly magnitudes are observed near 30°E and 75°W owing to the topographic barriers there (the East African highlands and the Andes, respectively) that are mostly higher than that of the 850-hPa pressure surface.

In comparison to the wind field, which propagates westward, the observed precipitation anomalies appear to be stationary in space with the magnitude of the anomalies changing as the wave propagates westward. As with King et al. (2015), the strongest and most extensive anomalies appear over the Gulf of Guinea and the tropical Andes, off the eastern coast of Colombia, and slightly east of the date line (180°). Smaller signals appear off the west coast of Sumatra and both coasts of the Philippines.

Observed precipitation over the Gulf of Guinea and near the date line is in quadrature with the wind anomalies, with enhanced precipitation leading westerly wind anomalies. However, over the tropical Andes, enhanced precipitation is roughly in phase with easterly wind anomalies and off the coast of Sumatra is roughly in phase with westerly wind anomalies. These precipitation composite anomalies and phase relative to the zonal wind anomalies are similar to those observed in outgoing longwave radiation, another convective proxy, particularly for the strong signals over the Gulf of Guinea and the Andes (King et al. 2015).

In line with the generally good representation of upper- and lower-tropospheric wind correlations associated with the 5-day wave in climate models, all the climate models accurately simulate the wavenumber-1 structure in horizontal winds, as demonstrated for three models in Fig. 5, albeit with higher-magnitude wind anomalies than seen in the observations. Most models represent the reduction in wind anomalies at 30°E, but fewer models well represent the reduction in amplitudes at 75°W, with higher-resolution models more likely to simulate reduced amplitudes at this location (see supplemental material for composites for all models).

All the models also have areas of statistically significant local precipitation anomalies, but the location, magnitude and significance of these anomalies vary and no model comes close to fully replicating the precipitation anomalies seen in the observational data. Despite this, the significant observed 5-day-wave-related precipitation anomalies over the Gulf of Guinea and West Africa are also present to some extent in all climate models investigated except GFDL-ESM2G and GFDL-ESM2M. These anomalies vary in extent from being highly localized near the islands of Bioko and Principe (roughly 0°–5°N, 7.5°E), like in MPI-ESM-P in Figs. 5a,b, to including a large amount of the Congo basin as represented in the ACCESS1.3 model (Figs. 5c,d) or a large east–west extent of the gulf as represented in INM-CM4.0 (Figs. 5e,f). While these models all represent some significant anomaly in the region, none well represent the strong land–sea contrast in anomalies seen in observations (Fig. 4).

Compared to the Gulf of Guinea and West Africa signals, the examined models perform less well in the Andean region, with a significant rainfall–wave interaction not present in nine of the climate models: BNU-ESM, CanESM2, CMCC-CESM, FGOALS-g2,

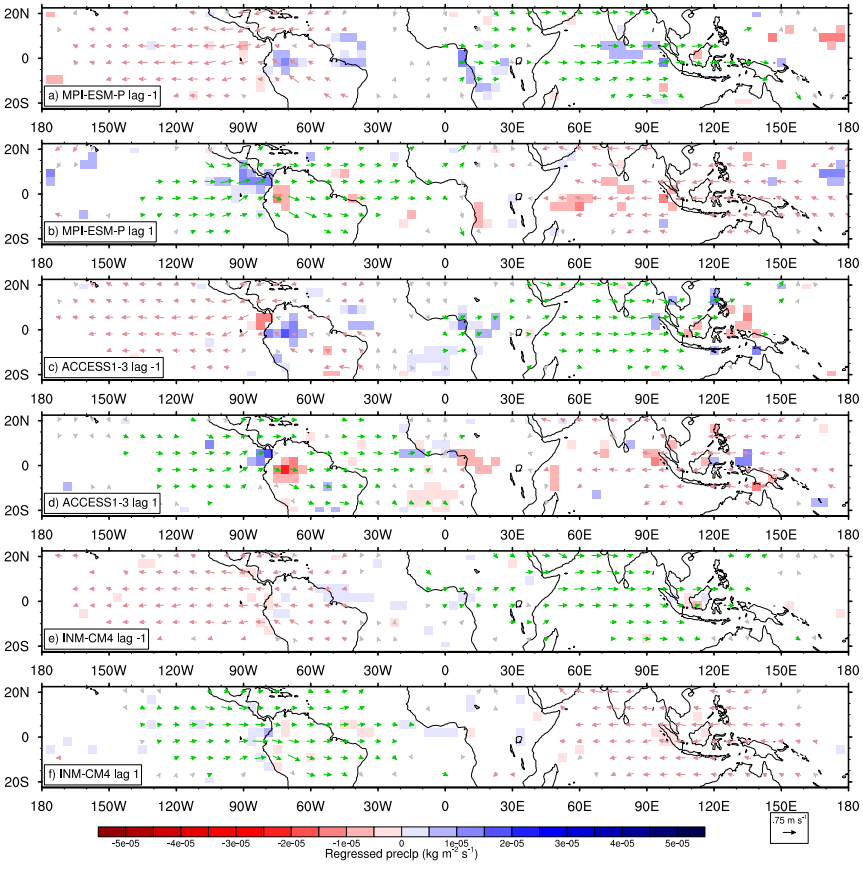

FIG. 5. Composite 850-hPa horizontal wind (vectors) and precipitation anomalies (shading) associated with the 5-day wave from three climate models: (a),(b) MPI-ESM-P, (c),(d) ACCESS1.3, and (e),(f) INM-CM4.0, at 1 day (a),(c),(e) before and (b),(d),(f) after maximum wave amplitude at 0°, 0°. Values are scaled by two standard deviations of wave amplitude. Values shown are significant at the 95% level.

GFDL CM3, GFDL-ESM2G, GFDL-ESM2M, IPSL-CM5A-LR, and IPSL-CM5B-LR.

Despite most models having significant precipitation anomalies at the 95% level in the areas of the strongest anomalies in observations, the magnitude of the model anomalies are in general lower than that observed in TRMM data. Figure 6 shows the pointwise variance in regressed precipitation between lags of −10 days to 10 days for all models averaged between 10°N and 10°S, with no models having a variance peak over the Gulf of Guinea greater than a quarter of that seen in TRMM data. The CMCC-CM, MPI-ESM-P, and MIROC4h models have the strongest anomaly variance directly over the Gulf of Guinea, with other models with strong variance in the region having their precipitation signals farther to the east, either at the West African coast (BCC_CSM1.1 and IPSL-CM5B-LR) or over the Congo basin [BCC_CSM1.1(m) and MIROC4h]. Model variances are closer to observations over the Andes, with CMCC-CM, BCC_CSM1.1, and MRI-ESM1 having strong regressed precipitation variance directly over the Andes, which is at least half that of the observations. The precipitation signals for most models are constrained more to the western edge of the Andes; however, the observed precipitation occurs primarily over the eastern edge of the Andes and the Amazonian foothills, which is only strongly apparent in BCC_CSM1.1(m), CMCC-CMS, MIROC4h, and MRI-CGCM3. Despite not being as strong as the associated precipitation over the Andes and West Africa, the observed precipitation variance over the Indian Ocean and western Pacific Ocean between 45°E and 150°W is matched by elevated precipitation variance in most of the models, with BCC_CSM1 and BCC_CSM1.1(m) having variance in this region very close to observations.

Over the tropical Andes, a relationship exists between model 5-day-wave precipitation anomaly magnitudes and the native longitudinal resolution of the climate

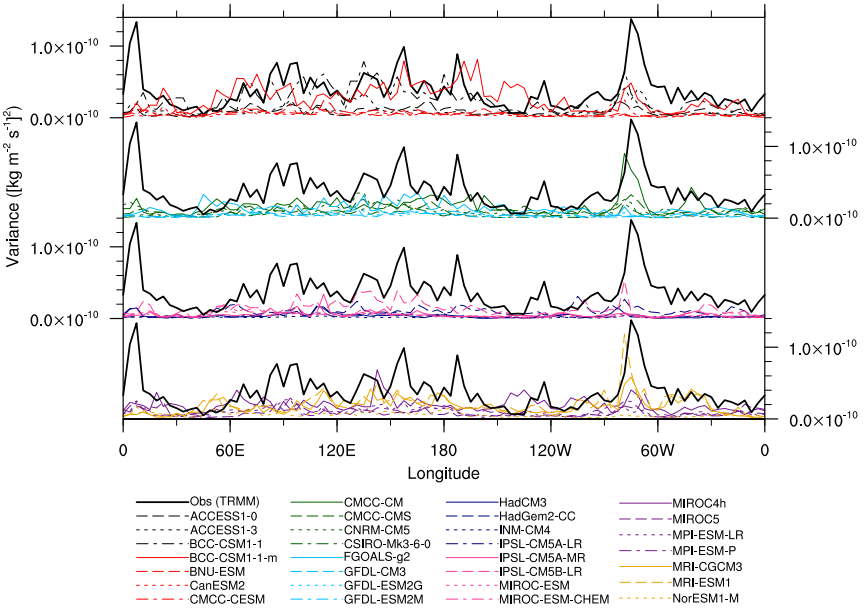

FIG. 6. Average between 10°N and 10°S of pointwise regressed composite precipitation variance over lags −10 to 10 days for the CMIP5 models and observations.

model, as is shown in the scatterplot in Fig. 7a. The R^2 value between the number of longitudinal grid points and variance of precipitation anomalies is 0.54, which is significant at above the 99% level. However, this relationship between model resolution and precipitation anomaly magnitudes does not hold for anomalies over the Gulf of Guinea, as can be seen in Fig. 7b. Here, there is only a very weak R^2 value of 0.08.

Comparisons between the model coherence-squared between precipitation and zonal winds (Fig. 3) and the 5-day-wave precipitation anomalies over the Gulf of Guinea and Andean regions are examined in Fig. 8. In

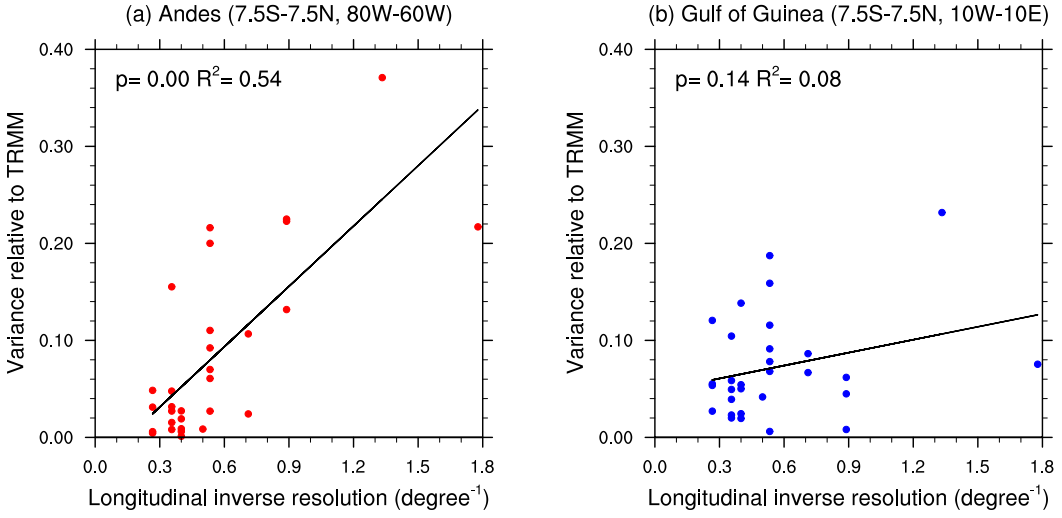

FIG. 7. Scatterplots of the regressed model precipitation variance relative to that shown in TRMM 3B42 against the native longitudinal resolution of the model (inverse degrees). The precipitation variances are calculated from averages for each lag calculated for a box over (a) the tropical Andes and (b) the Gulf of Guinea. Improved variance with increasing resolution explains over half of the observed variation in the region over the Andes, and the observed trend is statistically significant to no trend at above the 99% level. A much weaker and less significant trend is observed over the Gulf of Guinea.

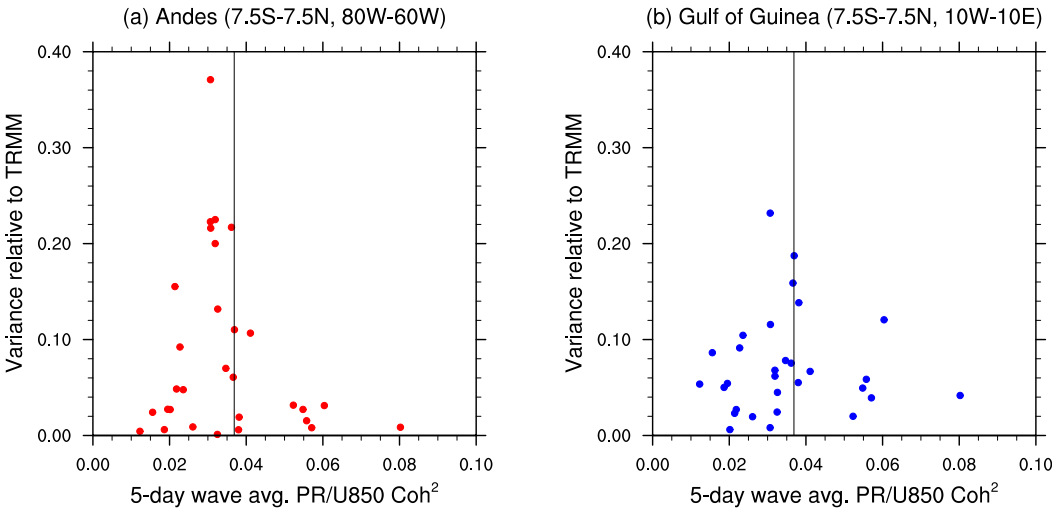

FIG. 8. Scatterplots of regressed model precipitation variance relative to that shown in TRMM 3B42 against the model coherence squared between precipitation and 850-hPa zonal wind averaged over the 5-day-wave range over (a) the tropical Andes and (b) the Gulf of Guinea. The vertical line marks the average coherence squared between precipitation and 850-hPa zonal wind in the 5-day-wave range observed in the reanalysis.

both the Andean and Gulf of Guinea regions, a relationship between the absolute magnitude of the model's difference from the observed spectral coherence-squared and model anomaly magnitude is seen, which is significant at more than a 90% level, but with small correlation coefficients (0.2 and 0.11, respectively). This suggests that models with better anomaly magnitudes are more likely to exhibit close spectral characteristics to observations, but conversely spectral characteristics close to observations are not a strong predictor of good anomaly magnitude simulation.

4. Discussion

Both the regressed composites and, to a lesser extent, the spectral coherences, have shown that while the CMIP5 climate models perform very well at simulating the dry dynamics of the 5-day wave, they are less able to accurately simulate its interaction with tropical convection. This runs somewhat counter to what is observed for the CCEWs and the MJO, for which the simulation of the dynamical fields is related to the simulation of the convective anomalies; in many models the MJO and CCEW simulation is poor in both the winds and convection.

This separation between the simulation quality of the dynamics and convective anomalies of the 5-day wave is informative about the nature of the 5-day wave and its observed interaction with convection. The current understanding of the observed waves is that disturbances in the atmosphere outside of those in the 5-day range force the wave, either through interactions with topography (Cheong and Kimura 1997) or through tropical convection on other time and length scales projecting upon the 5-day wave and thus driving it (Salby and Garcia 1987; Garcia and Salby 1987). Furthermore, model studies have shown that dry GCMs are able to generate Rossby–Haurwitz waves without the presence of moist convection and topography but with forcing for the wave coming from horizontal and vertical temperature gradients (Miyoshi and Hirooka 1999; Potter et al. 2014). These forcing mechanisms are likely active in the CMIP5 models and could drive 5-day-wave magnitudes in model winds close to observations even when the wave-associated convection in models is much lower than that observed in reanalysis data. Furthermore, if tropical convection anomalies on the spatial and temporal scale observed were a key factor in the forcing of the 5-day wave, one would expect the wind anomalies to be stronger in models with stronger precipitation anomalies. However, this is not what is observed with the model composites. Consequently, this implies that the observed 5-day-wave-related convective anomalies are not a major factor in the forcing and maintenance of the wave in both observations and models and that the association of tropical convection with the 5-day wave is due to the wave modulating convection.

The similarities between the 5-day-wave zonal wind coherences with precipitation in the models and in observations seem to run counter to the reduced model composite precipitation anomalies relative to the observations. However, this may be due to the 5-day wave

modulating a similar proportion of the total tropical convection in the models as in observations but that the level of total tropical convection at this temporal and spatial scale is reduced in the models. This is evident in the power spectra of precipitation in the climate models, which have reduced variance at the space and time scales of the 5-day wave relative to that seen in observations (Fig. 1). The increased variance in model zonal winds compared to observations at the spatial and temporal scales of the 5-day wave also explains the generally increased magnitude of wind anomalies in the model composites compared to the reanalysis.

The difficulties some models have with the 5-day-wave wind and precipitation amplitudes near the Andes are likely due to the differences in representation of Andean topography in the models. The near-equatorial Andes are tall and thin (~200-km wide and at least 4000 m in maximum elevation in an east–west transect). The width of the Andes, being around 1.8° of longitude, is close to and in many cases smaller than the longitudinal resolution of the models and as such lower resolution models are likely to smooth out the sharp barrier of the Andes. This will lead to increased 850-hPa wind anomalies in lower-resolution models, as the smoother terrain is lower than the 850-hPa pressure surface, and reduced precipitation anomalies, as a lower elevation barrier reduces the strength of the orographic effect postulated to be behind the 5-day-wave-related precipitation there (King et al. 2015). These effects would also explain why improved resolution does not strongly influence model precipitation anomalies over the Gulf of Guinea. It is hypothesized in King et al. (2015) that the rainfall associated with the 5-day wave there is not due to orographic interactions, and thus there is no strong reason to expect a relationship between resolution and wave-related rainfall in that region.

5. Conclusions

This study investigates the simulation of the interaction between the 5-day wave and tropical convection in 30 CMIP5 models. The model results are compared with an observational representation of the interaction determined from ERA-Interim and TRMM 3B42 rainfall estimates.

Spectral coherence-squared measurements between lower- and upper-tropospheric zonal winds show that all models have a strong dry dynamical signal corresponding to the $n = 1$ Rossby–Haurwitz waves. This agrees with previous studies showing that the $n = 1$ Rossby–Haurwitz waves exist as a well-resolved feature in numerical climate models and further suggests that the simulation of the basic dynamics are mainly independent of the quality of the simulated interaction with convection.

Significant spectral coherence between 850-hPa zonal winds and precipitation exists for all the investigated models in the 5-day wave range but with the coherence and peak period of this interaction between precipitation and zonal winds varying in the models around the magnitude of the observed coherence and peak period. The model spectral coherences for the 5-day wave are close to those in observations even when the models do not well simulate other large-scale wave interactions with convection in the tropics.

Lagged-regression composites tend to show that the models are very good at replicating the horizontal wind field associated with the 5-day wave. This is consistent with the spectral coherences between the upper and lower troposphere being close to observed and previous investigation of Rossby–Haurwitz wave dynamics in climate models.

The models do less well at identifying the spatial pattern of 5-day-wave-related precipitation anomalies. Despite most models having significant anomalies near the Gulf of Guinea and two-thirds having anomalies near the Andes, the spatial extent of the anomalies in the models does not exactly match that of observations, and the magnitude of the precipitation anomalies in these regions are too low by at least a factor of 3.

The magnitude of wave-related precipitation anomalies over the slopes of the Andes is significantly related to model resolution, with over half of the variation in the models' performance in this region coming from the changes in resolution, likely owing to improved orography in these models. However, this relationship does not hold over the Gulf of Guinea because, although there is a trend of increasing anomaly magnitude with increasing resolution, this trend is not statistically significant and explains little of the variation in model performance.

The reduced magnitude of 5-day-wave-related precipitation anomalies relative to observations in the models can be explained in light of similar wind field magnitudes and wind–precipitation coherence values by the models having reduced background variability of precipitation at the 5-day-wave scales. This is part of the redder precipitation spectra observed in the models, with higher variability at long periods and reduced variability at shorter periods.

Overall, the evidence suggests that the simulated interaction between the 5-day wave and tropical precipitation is mostly one way only, with the wave dynamics forcing the precipitation variations on the 5-day time scale. Given that the interaction over the Andes is consistent with orographic forcing, further efforts to

identify the mechanisms behind the interaction in the West African region will provide greater insight into the nature of the 5-day-wave modulation of tropical convection.

Acknowledgments. ERA-Interim data used in this study were provided by ECMWF and obtained from the ECMWF data server, and TRMM data were obtained from the NASA Goddard Earth Sciences (GES) Data and Information Services Center (DISC). This study was supported by the Australian Research Council's Centres of Excellence scheme (Grant CE110001028) and by an Australian Postgraduate Award for the first author. Research was undertaken with the assistance of resources from the National Computational Infrastructure (NCI) facility, which is supported by the Australian government. The authors acknowledge the World Climate Research Programme's Working Group on Coupled Modelling, which is responsible for CMIP, and thank the climate modeling groups for producing and making available their model output. The U.S. Department of Energy's Program for Climate Model Diagnosis and Intercomparison provides coordinating support for CMIP and led development of software infrastructure in partnership with the Global Organization for Earth System Science Portals. The authors also thank Jorgen Frederiksen, Hongyan Zhu, Stefan Tulich, and two anonymous reviewers for their feedback and comments on the manuscript.

REFERENCES

Adachi, Y., and Coauthors, 2013: Basic performance of a new Earth system model of the Meteorological Research Institute (MRI-ESM1). *Pap. Meteor. Geophys.*, **64**, 1–19, doi:10.2467/mripapers.64.1.

Arora, V. K., and Coauthors, 2011: Carbon emission limits required to satisfy future representative concentration pathways of greenhouse gases. *Geophys. Res. Lett.*, **38**, L05805, doi:10.1029/2010GL046270.

Bentsen, M., and Coauthors, 2013: The Norwegian Earth System Model, NorESM1-M—Part 1: Description and basic evaluation of the physical climate. *Geosci. Model Dev.*, **6**, 687–720, doi:10.5194/gmd-6-687-2013.

Bessafi, M., and M. C. Wheeler, 2006: Modulation of south Indian Ocean tropical cyclones by the Madden–Julian oscillation and convectively coupled equatorial waves. *Mon. Wea. Rev.*, **134**, 638–656, doi:10.1175/MWR3087.1.

Bi, D., and Coauthors, 2013: The ACCESS coupled model: Description, control climate and evaluation. *Aust. Meteor. Oceanogr. J.*, **63**, 41–64.

Burpee, R. W., 1976: Some features of global-scale 4–5 day waves. *J. Atmos. Sci.*, **33**, 2292–2299, doi:10.1175/1520-0469(1976)033<2292:SFOGSD>2.0.CO;2.

Cheong, H.-B., and R. Kimura, 1997: Excitation of the 5-day wave by Antarctica. *J. Atmos. Sci.*, **54**, 87–102, doi:10.1175/1520-0469(1997)054<0087:EOTDWB>2.0.CO;2.

Collins, M., S. F. B. Tett, and C. Cooper, 2001: The internal climate variability of HadCM3, a version of the Hadley Centre Coupled Model without flux adjustments. *Climate Dyn.*, **17**, 61–81, doi:10.1007/s003820000094.

Dee, D. P., and Coauthors, 2011: The ERA-Interim reanalysis: Configuration and performance of the data assimilation system. *Quart. J. Roy. Meteor. Soc.*, **137**, 553–597, doi:10.1002/qj.828.

Donner, L., and Coauthors, 2011: The dynamical core, physical parameterizations, and basic simulation characteristics of the atmospheric component AM3 of the GFDL global coupled model CM3. *J. Climate*, **24**, 3484–3519, doi:10.1175/2011JCLI3955.1.

Dufresne, J.-L., and Coauthors, 2013: Climate change projections using the IPSL-CM5 Earth system model: From CMIP3 to CMIP5. *Climate Dyn.*, **40**, 2123–2165, doi:10.1007/s00382-012-1636-1.

Dunne, J. P., and Coauthors, 2012: GFDL's ESM2 global coupled climate–carbon Earth system models. Part I: Physical formulation and baseline simulation characteristics. *J. Climate*, **25**, 6646–6665, doi:10.1175/JCLI-D-11-00560.1.

ECMWF, 2009: ERA-Interim Project. Meteorological Archival and Retrieval System, accessed 29 August 2014. [Available online at http://apps.ecmwf.int/datasets/data/interim-full-daily/.]

Elbern, H., and P. Speth, 1993: Energy of Rossby waves as a part of global atmospheric oscillations. *Tellus*, **45A**, 168–192, doi:10.1034/j.1600-0870.1993.t01-2-00002.x.

Garcia, R. R., and M. L. Salby, 1987: Transient response to localized episodic heating in the tropics. Part II: Far-field behavior. *J. Atmos. Sci.*, **44**, 499–532, doi:10.1175/1520-0469(1987)044<0499:TRTLEH>2.0.CO;2.

Giorgetta, M. A., and Coauthors, 2013: Climate and carbon cycle changes from 1850 to 2100 in MPI-ESM simulations for the Coupled Model Intercomparison Project phase 5. *J. Adv. Model. Earth Syst.*, **5**, 572–597, doi:10.1002/jame.20038.

Hamilton, K., 1987: General circulation model simulation of the structure and energetics of atmospheric normal modes. *Tellus*, **39A**, 435–459, doi:10.1111/j.1600-0870.1987.tb00320.x.

Hayashi, Y., and D. G. Golder, 1983: Transient planetary waves simulated by GFDL spectral general circulation models. Part I: Effects of mountains. *J. Atmos. Sci.*, **40**, 941–950, doi:10.1175/1520-0469(1983)040<0941:TPWSBG>2.0.CO;2.

Hendon, H. H., and B. Liebmann, 1990: The intraseasonal (30–50 day) oscillation of the Australian summer monsoon. *J. Atmos. Sci.*, **47**, 2909–2924, doi:10.1175/1520-0469(1990)047<2909:TIDOOT>2.0.CO;2.

——, and M. C. Wheeler, 2008: Some space–time spectral analyses of tropical convection and planetary-scale waves. *J. Atmos. Sci.*, **65**, 2936–2948, doi:10.1175/2008JAS2675.1.

Huffman, G. J., and Coauthors, 2007: The TRMM Multisatellite Precipitation Analysis (TMPA): Quasi-global, multiyear, combined-sensor precipitation estimates at fine scales. *J. Hydrometeor.*, **8**, 38–55, doi:10.1175/JHM560.1.

Hung, M.-P., J.-L. Lin, W. Wang, D. Kim, T. Shinoda, and S. J. Weaver, 2013: MJO and convectively coupled equatorial waves simulated by CMIP5 climate models. *J. Climate*, **26**, 6185–6214, doi:10.1175/JCLI-D-12-00541.1.

Ji, D., and Coauthors, 2014: Description and basic evaluation of Beijing Normal University Earth System Model (BNU-ESM) version 1. *Geosci. Model Dev.*, **7**, 2039–2064, doi:10.5194/gmd-7-2039-2014.

Jones, C., 2000: Occurrence of extreme precipitation events in California and relationships with the Madden–Julian oscillation. *J. Climate*, **13**, 3576–3587, doi:10.1175/1520-0442(2000)013<3576:OOEPEI>2.0.CO;2.

Kasahara, A., 1980: Effect of zonal flows on the free oscillations of a barotropic atmosphere. *J. Atmos. Sci.*, **37**, 917–929, doi:10.1175/1520-0469(1980)037<0917:EOZFOT>2.0.CO;2.

Kiladis, G. N., M. C. Wheeler, P. T. Haertel, K. H. Straub, and P. E. Roundy, 2009: Convectively coupled equatorial waves. *Rev. Geophys.*, **47**, RG2003, doi:10.1029/2008RG000266.

King, M. J., M. C. Wheeler, and T. P. Lane, 2015: Association of convection with the 5-day Rossby–Haurwitz wave. *J. Atmos. Sci.*, **72**, 3309–3321, doi:10.1175/JAS-D-14-0316.1.

Liebmann, B., H. H. Hendon, and J. D. Glick, 1994: The relationship between tropical cyclones of the western Pacific and Indian Oceans and the Madden-Julian oscillation. *J. Meteor. Soc. Japan*, **72**, 401–411.

Lin, J.-L., and Coauthors, 2006: Tropical intraseasonal variability in 14 IPCC AR4 climate models. Part I: Convective signals. *J. Climate*, **19**, 2665–2690, doi:10.1175/JCLI3735.1.

Lott, F., and Coauthors, 2014: Kelvin and Rossby-gravity wave packets in the lower stratosphere of some high-top CMIP5 models. *J. Geophys. Res. Atmos.*, **119**, 2156–2173, doi:10.1002/2013JD020797.

Madden, R. A., 2007: Large-scale, free Rossby waves in the atmosphere—an update. *Tellus*, **59A**, 571–590, doi:10.1111/j.1600-0870.2007.00257.x.

——, and P. Julian, 1972a: Description of global-scale circulation cells in the tropics with a 40–50 day period. *J. Atmos. Sci.*, **29**, 1109–1123, doi:10.1175/1520-0469(1972)029<1109:DOGSCC>2.0.CO;2.

——, and ——, 1972b: Further evidence of global-scale, 5-day pressure waves. *J. Atmos. Sci.*, **29**, 1464–1469, doi:10.1175/1520-0469(1972)029<1464:FEOGSD>2.0.CO;2.

Manzini, E., and K. Hamilton, 1993: Middle atmospheric traveling waves forced by latent and convective heating. *J. Atmos. Sci.*, **50**, 2180–2200, doi:10.1175/1520-0469(1993)050<2180:MATWFB>2.0.CO;2.

Martin, G., and Coauthors, 2011: The HadGEM2 family of Met Office Unified Model climate configurations. *Geosci. Model Dev.*, **4**, 723–757, doi:10.5194/gmd-4-723-2011.

Miyoshi, Y., and T. Hirooka, 1999: A numerical experiment of excitation of the 5-day wave by a GCM. *J. Atmos. Sci.*, **56**, 1698–1707, doi:10.1175/1520-0469(1999)056<1698:ANEOEO>2.0.CO;2.

Potter, S. F., G. K. Vallis, and J. L. Mitchell, 2014: Spontaneous superrotation and the role of Kelvin waves in an idealized dry GCM. *J. Atmos. Sci.*, **71**, 596–613, doi:10.1175/JAS-D-13-0150.1.

Rotstayn, L., M. Collier, Y. Feng, H. Gordon, S. O'Farrell, I. Smith, and J. Syktus, 2010: Improved simulation of Australian climate and ENSO-related rainfall variability in a global climate model with an interactive aerosol treatment. *Int. J. Climatol.*, **30**, 1067–1088, doi:10.1002/joc.1952.

Sakamoto, T. T., and Coauthors, 2012: MIROC4h—A new high-resolution atmosphere-ocean coupled general circulation model. *J. Meteor. Soc. Japan*, **90**, 325–359, doi:10.2151/jmsj.2012-301.

Salby, M. L., 1984: Survey of planetary-scale travelling waves: The state of theory and observations. *Rev. Geophys.*, **22**, 209–236, doi:10.1029/RG022i002p00209.

——, and R. R. Garcia, 1987: Transient response to localized episodic heating in the tropics. Part I: Excitation and short-time near-field behavior. *J. Atmos. Sci.*, **44**, 458–498, doi:10.1175/1520-0469(1987)044<0458:TRTLEH>2.0.CO;2.

Scoccimarro, E., and Coauthors, 2011: Effects of tropical cyclones on ocean heat transport in a high-resolution coupled general circulation model. *J. Climate*, **24**, 4368–4384, doi:10.1175/2011JCLI4104.1.

Straub, K. H., P. T. Haertel, and G. N. Kiladis, 2010: An analysis of convectively coupled Kelvin waves in 20 WCRP CMIP3 global coupled climate models. *J. Climate*, **23**, 3031–3056, doi:10.1175/2009JCLI3422.1.

TRMM, 2011: TRMM (TMPA) Rainfall estimate L3 3 hour 0.25 degree × 0.25 degree, version 7. NASA Goddard Earth Sciences Data and Information Services Center, accessed 30 May 2014. [Available online at http://disc.gsfc.nasa.gov/datacollection/TRMM_3B42_7.html.]

Voldoire, A., and Coauthors, 2013: The CNRM-CM5.1 global climate model: Description and basic evaluation. *Climate Dyn.*, **40**, 2091–2121, doi:10.1007/s00382-011-1259-y.

Volodin, E., N. Dianskii, and A. Gusev, 2010: Simulating present-day climate with the INMCM4.0 coupled model of the atmospheric and oceanic general circulations. *Izv., Atmos. Oceanic Phys.*, **46**, 414–431, doi:10.1134/S000143381004002X.

von Storch, H., and F. W. Zwiers, 1999: *Statistical Analysis in Climate Research.* Cambridge University Press, 484 pp.

Watanabe, M., and Coauthors, 2010: Improved climate simulation by MIROC5: Mean states, variability, and climate sensitivity. *J. Climate*, **23**, 6312–6335, doi:10.1175/2010JCLI3679.1.

Williamson, D. L., J. B. Drake, J. J. Hack, R. Jakob, and P. N. Swarztrauber, 1992: A standard test set for numerical approximations to the shallow water equations in spherical geometry. *J. Comput. Phys.*, **102**, 211–224, doi:10.1016/S0021-9991(05)80016-6.

Xin, X.-G., T.-W. Wu, and J. Zhang, 2013: Introduction of CMIP5 experiments carried out with the climate system models of Beijing Climate Center. *Adv. Climate Change Res.*, **4**, 41–49, doi:10.3724/SP.J.1248.2013.00041.

Yasunaga, K., and B. Mapes, 2012: Differences between more divergent and more rotational types of convectively coupled equatorial waves. Part I: Space–time spectral analyses. *J. Atmos. Sci.*, **69**, 3–16, doi:10.1175/JAS-D-11-033.1.

Yasunari, T., 1979: Cloudiness fluctuations associated with the Northern Hemisphere summer monsoon. *J. Meteor. Soc. Japan*, **57**, 227–242.

Yukimoto, S., and Coauthors, 2012: A new global climate model of the Meteorological Research Institute: MRI-CGCM3—Model description and basic performance. *J. Meteor. Soc. Japan*, **90A**, 23–64, doi:10.2151/jmsj.2012-A02.

Zhang, C., 2005: Madden-Julian oscillation. *Rev. Geophys.*, **43**, RG2003, doi:10.1029/2004RG000158.

Zhou, T., F. Song, and X. Chen, 2013: Historical evolution of global and regional surface air temperature simulated by FGOALS-s2 and FGOALS-g2: How reliable are the model results? *Adv. Atmos. Sci.*, **30**, 638–657, doi:10.1007/s00376-013-2205-1.